Proceedings of the International Symposium on Physics of Materials (ISPMA 14), September 10–15, 2017, Prague

Preparation of Fe–Al–Si Intermetallic Compound by Mechanical Alloying and Spark Plasma Sintering

P. Haušild[a*], M. Karlík[a,b], J. Čech[a], F. Průša[c], K. Nová[c], P. Novák[c], P. Minárik[b] and J. Kopeček[d]

[a]Czech Technical University in Prague, Faculty of Nuclear Sciences and Physical Engineering, Department of Materials, Trojanova 13, 120 00 Prague 2, Czech Republic

[b]Charles University, Department of Physics of Materials, Ke Karlovu 5, 121 16 Prague 2, Czech Republic

[c]University of Chemistry and Technology Prague, Department of Metals and Corrosion Engineering, Technická 5, 166 28 Prague 6, Czech Republic

[d]Institute of Physics, ASCR, v.v.i., Department of Functional Materials, Na Slovance 2, 18221 Prague 8, Czech Republic

The effect of processing conditions on microstructure and mechanical properties of mechanically alloyed Fe20Al20Si (wt%) intermetallic compound was examined. The microstructure, phase composition and mechanical properties after various durations of mechanical alloying were characterized and optimum conditions of mechanical alloying were used for spark plasma sintering. Spark plasma sintering parameters were also optimised so that correctly sintered samples preserved phase composition and mechanical properties of milled powders.

DOI: 10.12693/APhysPolA.134.724

PACS/topics: 81.05.Bx, 81.20.Ev, 46.55.+d

1. Introduction

Future possible shortage of crucial/essential elements such as chromium raises the effort to develop materials that may replace or even outperform the currently available stainless steels or nickel superalloys. Among currently investigated materials, the iron-based intermetallics are the most promising materials [1–3]. Ternary Fe–Al–Si alloys show quite unique properties e.g. excellent corrosion properties in oxidizing and sulfidizing environment, high-temperature oxidation resistance and wear resistance [4]. However, these alloys exhibit difficulties with conventional routes of processing such as casting and hot and/or cold rolling.

Interesting way of processing could therefore be mechanical alloying (MA) which starts from blended elemental powder mixtures and allows production of homogeneous materials by severe deformation in a high-energy ball charge [5]. Mechanical alloying involves repeated cold welding, fracturing and rewelding of a mixture of powder particles and allows to produce a controlled, extremely fine microstructure. However, subsequent sintering of powders at high temperature and long annealing time can lead to grain coarsening or even to alloy decomposition into thermodynamically more stable phases [6].

For this reason, it is convenient to use spark plasma sintering (SPS) [7, 8] as this method leads to high rates of densification whereas grain coarsening is suppressed due to the short processing time (heating rates are much higher than that of e.g. hot isostatic pressing).

*corresponding author; e-mail: Petr.Hausild@fjfi.cvut.cz

In this work, the effect of processing conditions on microstructure and mechanical properties of Fe–Al–Si alloys is presented and discussed. The microstructure and mechanical properties during each step of processing consisting of mechanical alloying and spark plasma sintering are characterized by means of light microscopy, scanning electron microscopy (SEM), transmission electron microscopy (TEM), energy dispersive X-ray spectroscopy (EDS), X-ray diffraction (XRD), differential scanning calorimetry (DSC) and micro/nano hardness measurements.

2. Experimental details

2.1. Mechanical alloying

Composition of the alloy was chosen as FeAl20Si20 wt% (42.5Fe–29.3Al–28.2Si at.%) in order to compare the microstructure and properties with alloy previously prepared by reactive sintering [9]. The feedstock material for mechanical alloying consisted of Al (Strem Chemicals, purity of 99.7%), Si (Alfa Aesar, purity of 99.5%) and Fe (Strem Chemicals, purity of 99.9%) powders, which contained powder particles with average dimensions of 44 μm (Al and Si) and 9 μm (Fe), respectively. Powders were blended in appropriate amounts and placed into a steel mould together with milling balls. Both steel mould and milling balls were made of AISI 420 stainless steel. The mould was sealed and flushed for at least 5 min with argon to prevent undesirable oxidation during mechanical alloying in Retsch PM 100 device. The batches of 5 g and 20 g were processed in order to compare the effect of powder amount on MA kinetics. The ball-to-powder mass ratio

was set to be 1:60 for 5 g batches and 1:15 for 20 g batches, rotational speed was 400 rpm. The total duration of the process varied from 0.5 to 24 h. During the process, small amounts of mechanically alloyed powders were collected for metallographic and XRD analyses in order to determine the present phases and to describe the evolution of phase compositions as a function of the total time of the MA.

Microstructure of powders was characterized after various durations of mechanical alloying. The powder particles were embedded in the conductive resin and metallographically polished down to 0.04 μm colloidal silica suspension.

Microstructural observations were carried out by means of the metallographic microscope Neophot 32, JEOL JSM 5510LV scanning electron microscope equipped with iXRF 500 energy dispersive X-ray spectroscopy analyser and JEOL 2200FS transmission electron microscope. Phase composition was determined by a PANalytical X'Pert Pro X-ray diffractometer with Cu cathode in the Bragg–Brentano geometry. DSC analysis was performed on SETARAM multi-detector high temperature calorimeter MHTC-96.

Nanoindentation measurements were performed on Anton Paar NHT Nanoindentation Tester with Berkovich indenter using instrumented indentation technique [10, 11]. The results were evaluated according to the ISO 14577 standard [12]. Based on preliminary experiments, the load of 2 mN was chosen in order to be able to compare the hardness of individual mechanically alloyed powders (not affected by embedding resin) with the hardness of sintered samples. At least ten indentations were carried out (in the case of embedded powders in ten different particles) in order to obtain statistically representative results.

2.2. Spark plasma sintering

The MA powder was sintered into disc specimens having 20 mm in diameter and height of approximately 8 mm using a FCT Systeme HP D 10 device. The tool system placed inside the vacuum chamber consists of a graphite punch-and-die unit where the powders are loaded. Both punches are connected via graphite protection plates to electrodes. Graphite paper was used to prevent sticking between the loose powder and the graphite parts. During sintering process, the sample was compressed by a pressure of 50 MPa and heated by direct current (DC) by heating rate of 300 °C/min up to 900 °C and then by 100 °C/min to the sintering temperature (1000 °C) to minimize the sintering temperature overshoot. The total time the sample remained at sintering temperature was 10 min after which a slow cooling step with a cooling speed of 50 °C/min was set with simultaneous compaction pressure reduction till the sample reached temperature of 300 °C. The temperature of the compacting unit was measured by a pyrometer located above the punch-and-die unit. An extensive description of the equipment is given elsewhere [13].

Samples from SPS sinters were cut by low-speed diamond saw in the central part of the sintered cylinders, metallographically polished by standard procedure and characterized by methods described above.

3. Results and discussion

3.1. Mechanical alloying

Microstructure of powders was characterized after 0 h, 0.5 h, 1 h, 2 h, 3 h, 4 h, 6 h, 8 h, 10 h, and 24 h of milling (mechanical alloying). At the first stage of milling (during rapid fracturing and cold welding), convoluted lamellae can be observed within the particles. With increase of time of milling, lamellae get finer and more convoluted along with the beginning of dissolution (Fig. 1a). Almost complete solid solution formation (with only sporadic islands of undissolved initial powders – Fig. 1b) was observed after 4 h of milling in the case of 5 g batch whereas in the case of 20 g batch it took about 8–10 h. Energy dispersive X-ray spectroscopy revealed that extensive increasing of milling time (i.e. 24 h) led to contamination of powders by 1–2 wt% (0.75–1.5 at.%) of chromium probably from the milling vessel.

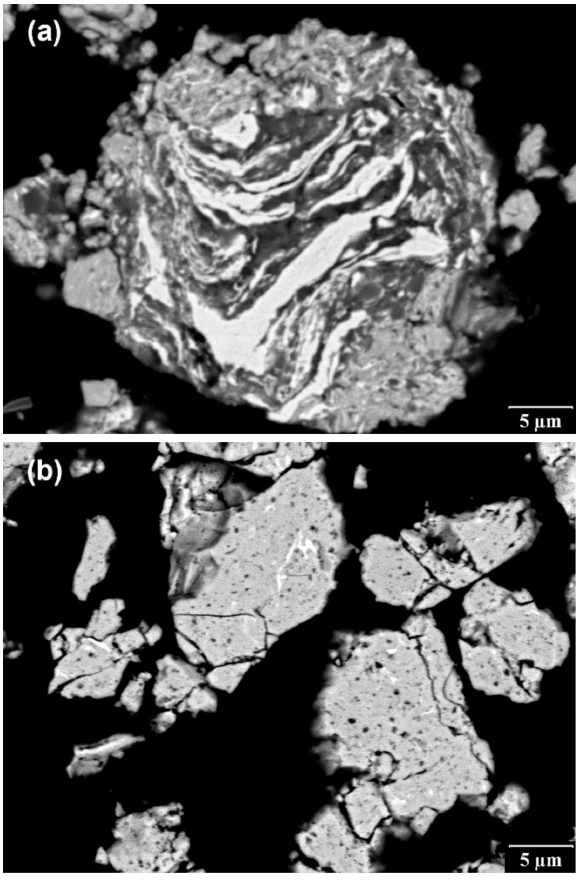

Fig. 1. Microstructure (SEM — backscattered electron signal) of mechanically alloyed powders from 20 g batch: (a) after 2 h of milling, (b) 10 h of milling.

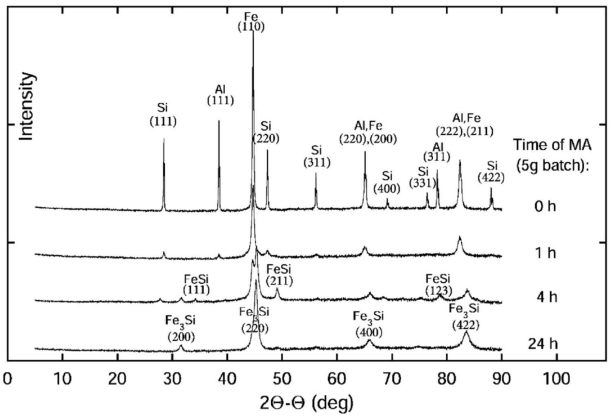

Fig. 2. XRD patterns of 5 g batch FeAlSi powder after various durations of milling.

In 5 g batch, X-ray diffraction unambiguously detected peaks corresponding to intermetallic phases after 2 h of milling; in the case of 20 g batch, the appearance of intermetallic phases was slightly delayed. With increase of time of milling, the amount of intermetallic phases gradually increased until the phase composition reached a mixture of Fe_3Si and FeSi (supersaturated by Al due to mechanical alloying — Fig. 2). Mechanical alloying led to peak shift and peak broadening, which can be attributed partly to the formation of supersaturated solid solution, significant grain refinement and the change in the lattice parameters induced by extensive deformation during MA.

TEM characterization was carried out on milled powder from 5g/4h and 20g/10h batches. Loose powders were deposited on copper grid with holey carbon film either in dry condition or from water suspension. In consequence, only smaller particles than 5 μm were examined. EDS in TEM revealed that for both 5 g and 20 g batches the chemical composition of these small particles was relatively uniform; the element content was in the range (wt%) 55 to 66% of Fe, 10 to 15% of Al, 13 to 16% of Si, and 0.7 to 4% of O (at.%: 40 to 54% of Fe, 18 to 24% of Al, 21 to 24% of Si, and 2 to 10% of O). Observed local differences in chemical composition are expectable in the case of mechanical alloying, because of the nature of this process.

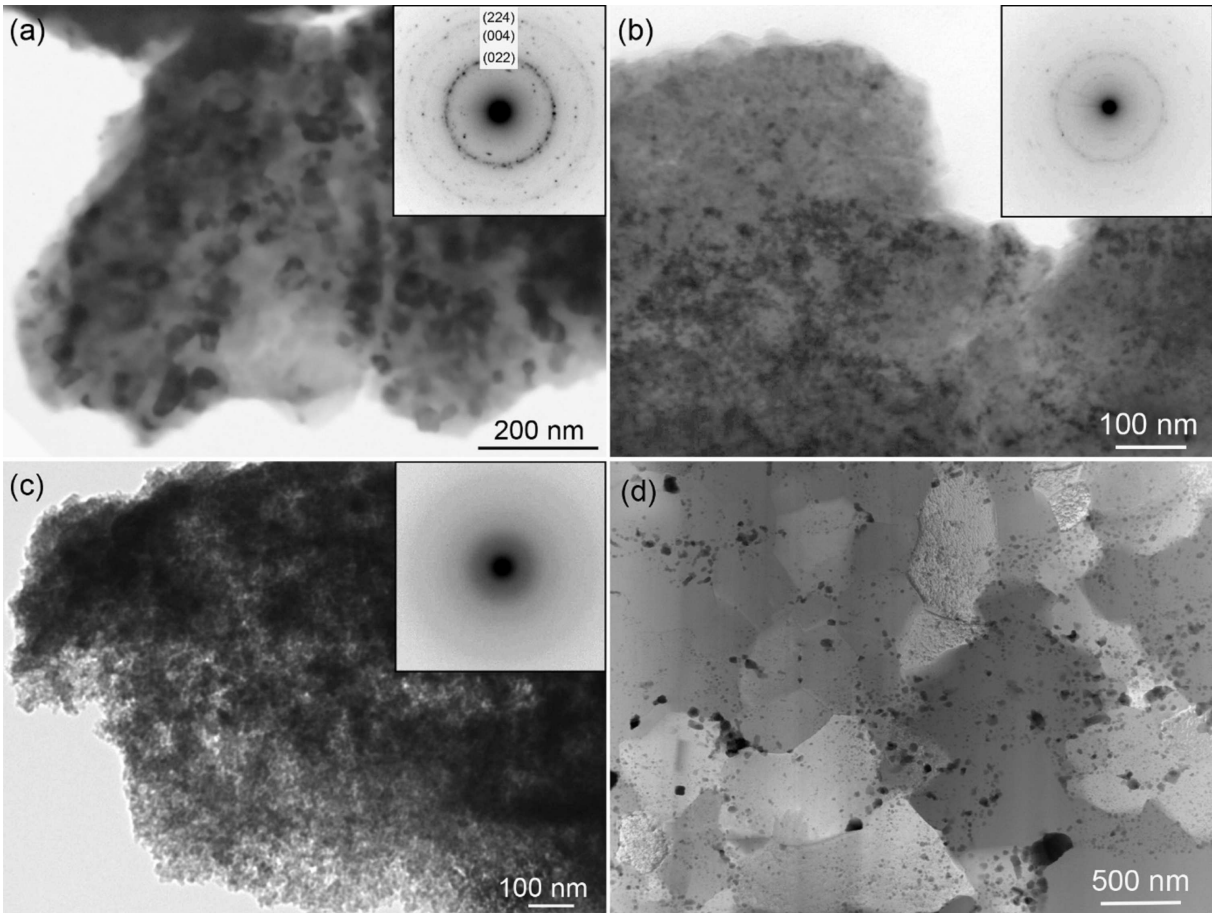

Fig. 3. TEM micrographs: (a) powder of the batch 5g/4h, the inset shows related diffraction pattern corresponding to the Fe_3Si phase, (b) crushed fragment from the 20g/10h_SPS material — nanocrystalline phase Fe_3Si, (c) crushed fragment from the 20g/10h_SPS material — amorphous nanoparticles, (d) STEM HAADF micrograph of a FIB lamella taken from 5g/4h_SPS material — fine grains and numerous oxide particles.

In the case of plastically deformable reactants, the mechanical alloying starts with the formation of lamellar structure (Fig. 1a). As the diffusion transport is limited during MA, the local variations in iron and aluminium content are obtained. In the case of silicon, the distribution is much more homogeneous, because brittle powder is crushed to very fine particles during the first stage of MA process and then it is easily distributed through the reaction mixture. The other factor, causing the nanoheterogeneity of the MA-produced powder, is the high level of mutual substitution of the elements in the obtained compounds, exceeding the equilibrium solubility limits [14, 15]. Therefore, the alternation of Fe and Si by Al can be observed in the silicide compound. It implies that the local heterogeneity cannot be fully avoided, but only minimized. Several Si-oxide particles were also found. Typical Fe-rich particle, agglomerate of very small grains, 20 to 100 nm in size, is presented in Fig. 3a. The diameters of the rings in the related electron diffraction pattern in the inset correspond to the Fe_3Si phase (Fm-$3m$, space group 225, $a = 0.5655$ nm). Under condensed electron beam, most of the particles melted and formed spherical droplets due to very high stored energy after MA.

Nanohardness of particles after milling showed an increasing trend with the milling time up to the stabilized value (plateau) for both 5 g and 20 g batches (see Fig. 4), In the beginning of milling, the particles in 5 g batch showed higher hardness than particles from 20 g batch; after about 4 h this trend was inversed. For 5 g batch, the plateau was reached after about 4 h; for 20 g batch, the plateau was reached after about 8 h. Slightly higher value of stabilized hardness after milling was obtained in the case of 20 g batch, which indicates the importance of milling parameters for the same compositions of powders.

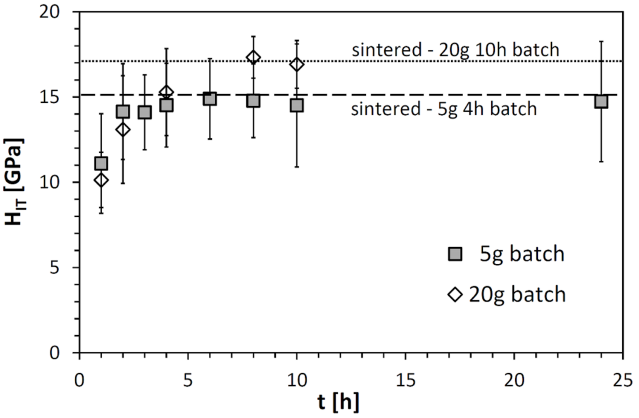

Fig. 4. Evolution of powder nanohardness as a function of time of milling (points with error bars) compared with nanohardness of sintered samples (dashed and dotted lines).

3.2. Spark plasma sintering

Based on the previous results obtained on mechanically alloyed powders after various durations of milling, optimum condition of MA for spark plasma sintering were chosen, i.e. powders milled 4 h (5 g batch) and/or 10 h (20 g batch). Sintering temperature was set according to DSC analysis of MA powders before first exothermic peak (occurring at about 1050 °C). The specimens were therefore sintered at 1000 °C (it was verified that lower sintering temperatures did not lead to fully compacted samples).

SEM and TEM characterization was carried out on sintered samples from both batches. The sintered materials were very brittle and so the easiest way to prepare a TEM sample was crushing in an agate mortar. It was found that SPS led to refining of the crystallites of the Fe_3Si phase (Fig. 3b), probably due to recrystallization. Furthermore, amorphous nanoparticles were identified (Fig. 3c), formed possibly due to liquid phase sintering and rapid cooling of the compact. These phases may be at the origin of the brittleness of the compact. According to EDS analysis, the chemical composition of the particles from the crushed compact was practically the same as of the loose MA powder, except of the oxygen content, which was in the range from 2.8 to 9.5 wt%. The presence of numerous oxide particles was confirmed during scanning transmission electron microscopy observation (Fig. 3d) using high angle annular dark field detector (STEM-HAADF) of a thin lamella prepared by focused ion beam (FIB). The micrograph in Fig. 3d shows mostly equiaxed grains from 200 nm to 1.5 μm in diameter and numerous oxide particles, from 10 nm up to 200 nm in size. Inside of some grains, dislocation networks were observed. No traces of initial pure powders were found in spark plasma sintered samples.

Measured nanohardness of SPS samples from milled powders was in a good agreement with hardness of milled powders (compare the values in Fig. 4), which means that mechanical properties were not significantly affected by pre-heating and heating during spark plasma sintering.

4. Summary

Microstructure and mechanical properties of mechanically alloyed Fe20Al20Si (wt%) intermetallic compound were examined during each step of processing.

The microstructure, phase composition and mechanical properties after various durations of mechanical alloying were characterized for two different powder amounts. Almost complete solid solution formation was reached after mechanical alloying. Optimum conditions of mechanical alloying were subsequently used for spark plasma sintering. Spark plasma sintering parameters were optimised so that correctly sintered samples preserved phase composition and mechanical properties of milled powders.

Acknowledgments

This research was carried out in the frame of the project 17-07559S (Czech Science Foundation) and of the project No. CZ.02.1.01/0.0/0.0/15_003/0000485, financed by ERDF.

References

[1] N.S. Stoloff, *Mater. Sci. Eng. A* **258**, 1 (1998).

[2] P. Kratochvíl, *Intermetallics* **16**, 587 (2008).

[3] P. Kratochvíl, M. Karlík, P. Haušild, M. Cieslar, *Intermetallics* **7**, 847 (1999).

[4] P. Novák, M. Zelinková, J. Šerák, A. Michalcová, M. Novák, D. Vojtěch, *Intermetallics* **19**, 1306 (2011).

[5] C. Suryanarayana, *Prog. Mater. Sci.* **46**, 1 (2001).

[6] H.K.D.H. Bhadeshia, *Mater. Sci. Technol.* **16**, 1404 (2000).

[7] R. Orrů, R. Licheri, A.M. Locci, A. Cincotti, G. Cao, *Mater. Sci. Eng. R* **63**, 127 (2009).

[8] T. Skiba, P. Haušild, M. Karlík, K. Vanmeensel, J. Vleugels, *Intermetallics* **18**, 1410 (2010).

[9] P. Novák, V. Knotek, J. Šerák, A. Michalcová, D. Vojtěch, *Powder Metall.* **54**, 167 (2011).

[10] W.C. Oliver, G.M. Pharr, *J. Mater. Res.* **7**, 1564 (1992).

[11] W.C. Oliver, G.M. Pharr, *J. Mater. Res.* **19**, 3 (2004).

[12] ISO 14577-1:2015, Instrumented indentation test for hardness and materials parameters — Part 1: Test method, ISO Standard, 2015.

[13] O. Guillon, J. Gonzalez-Julian, B. Dargatz, T. Kessel, G. Schierning, J. Räthel, M. Herrmann, *Adv. Eng. Mater.* **16**, 830 (2014).

[14] T.F. Grigorieva, A.P. Barinova, V. Boldyrev, E.Y. Ivanov, *Mater. Sci. Forum* **225-227**, 417 (1996).

[15] B.B. Khina, F.R. Froes, *JOM* **48**, 36 (1996).